

Cobalt(II) and silver(I) coordination polymers constructed from flexible bis(5,6-dimethylbenzimidazole) and substituted isophthalate co-ligands

Rui Yang · Kristof Van Hecke · Bao Yi Yu ·
Guang Yue Li · Guang Hua Cui

Received: 4 March 2014 / Accepted: 15 April 2014
© Springer International Publishing Switzerland 2014

Abstract Two coordination polymers, $[\text{Co}(\text{L1})(\text{IPA})_n$ (**1**) and $\{[\text{Ag}(\text{L2})(\text{HMIPA})]\cdot\text{H}_2\text{O}\}_n$ (**2**) (H_2IPA = isophthalic acid, L1 = 1,2-bis(5,6-dimethylbenzimidazol-1-yl)methyl) benzene, H_2MIPA = 5-methylisophthalic acid, L2 = 1,6-bis(5,6-dimethylbenzimidazol-1-yl)hexane, have been synthesized and characterized by physicochemical and spectroscopic methods, as well as single-crystal X-ray diffraction. In **1**, six-coordinated cobalt centers are bridged by L1 and IPA^{2-} ligands to generate a (4,4) two-dimensional layer. However, complex **2** features a 1D chain structure, which is further extended by $\text{O}\cdots\text{H}\cdots\text{O}$ hydrogen bonding interactions into a 2D supramolecular layer with (6³) topology. The fluorescence and thermal gravimetric analysis of both complexes were also explored. Furthermore, the complexes **1** and **2** exhibit remarkable catalytic properties for the degradation of methyl orange dyes in a Fenton-like process.

Introduction

In recent years, the rational design and synthesis of metal-organic coordination polymers (MOCPs) have received many researchers' attention, not least because of the profuse structures and fascinating topologies, but also for their potential applications as functional materials in catalysis, luminescence, magnetism and gas absorption [1–5]. It is well known that

construction of novel MOCPs depends on several factors, such as metal–ligand ratio, choice of solvents, pH of the solution, temperature, diversity of the ligands and possible supramolecular interactions [6–12]. Among these factors, N-donor ligands play a key role in the design and construction of such coordination polymers. The flexible bis(5,6-dimethylbenzimidazole) ligands have been given more and more attention by our and other groups [13–17], due to their strong coordination ability and the flexibility of the $-(\text{CH}_2)_n-$ or $-(\text{Ph}-\text{CH}_2)_n-$ spacer, which allow the ligands to bend and rotate in order to conform to the coordination geometries of the metal atoms and consequently generate more robust and intricate networks. Moreover, 5,6-dimethylbenzimidazole can serve as an axial ligand for cobalt in the biosynthesis of vitamin B₁₂ [18, 19]. In addition, aromatic polycarboxylates are excellent building units, and especially isophthalic acid and its derivatives serve as good candidates because of their various coordination modes [20–24]. The employment of mixed ligands of N-containing groups and dicarboxylates can compensate the charge balance, coordination deficiency, and weak interactions all at once, which enriches further the versatility of coordination complexes [25]. As a part of our continuing work on ternary metal complexes based on flexible bis(5,6-dimethylbenzimidazole) derivative and carboxylic acid ligands, herein, we report the syntheses and characterization of two new MOCPs, namely $[\text{Co}(\text{L1})(\text{IPA})_n$ (**1**) and $\{[\text{Ag}(\text{L2})(\text{HMIPA})]\cdot\text{H}_2\text{O}\}_n$ (**2**). Their thermal stabilities, luminescent and catalytic properties were investigated.

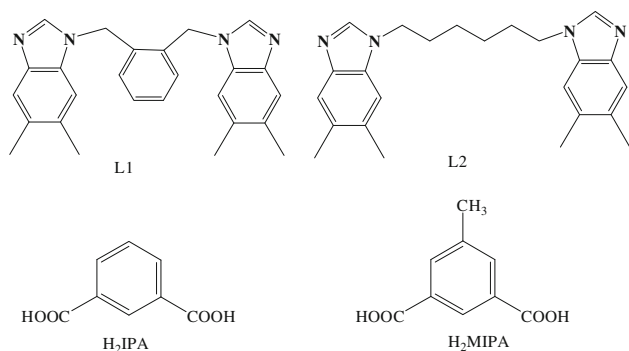
R. Yang · G. Y. Li · G. H. Cui (✉)
College of Chemical Engineering, Hebei United University,
46 West Xinhua Road, Tangshan 063009, Hebei,
People's Republic of China
e-mail: tscghua@126.com

K. Van Hecke · B. Y. Yu
Department of Inorganic and Physical Chemistry, Ghent
University, Krijgslaan 281 S3, 9000 Ghent, Belgium

Experimental

Materials and measurements

All the reagents and solvents used for the synthesis were commercially available and used directly without further



Scheme 1 Ligands L1, L2, H₂IPA and H₂MIPA

purification. The ligands L1 and L2 were synthesized according to a previously reported literature method [26] (Scheme 1). IR data were recorded on an Avatar 360 (Nicolet) spectrophotometer with KBr pellets in the region of 4,000–400 cm⁻¹. Elemental analyses of C, H and N were carried out on a Perkin-Elmer 240C automatic analyzer. Thermal analyses were performed on a Netzsch TG 209 thermal analyzer from room temperature to 800 °C under nitrogen atmosphere with a heating rate of 10 °C min⁻¹. The luminescence spectra for the powdered solid samples were measured at room temperature on a Hitachi F-7000 fluorescence spectrophotometer.

Synthesis of the [Co(L1)(IPA)]_n (**1**)

A mixture of Co(OAc)₂·4H₂O (24.9 mg, 0.1 mmol), L1 (39.4 mg, 0.1 mmol), H₂IPA (16.6 mg, 0.1 mmol) and H₂O (15 mL) was sealed in a 25 mL Teflon-lined stainless vessel and heated to 140 °C for 3 days under autogenous pressure. Afterward, the autoclave was cooled down to room temperature at a rate of 5 °C/h. Purple block-shaped crystals of **1** were isolated with a yield of 52 % (based on Co(OAc)₂·4H₂O). Calcd. for C₃₄H₃₀CoN₄O₄ (Fw = 617.55): C 66.1, H 4.9, N 9.1 %; found: C 65.8, H 5.1, N 9.4 %. FTIR (KBr pellet, cm⁻¹): 3,116 w, 2,930 w, 1,613 s, 1,563 s, 1,513 s, 1,433 s, 1,385 s, 1,060 m, 952 w, 832 w, 735 s.

Synthesis of the {[Ag(L2)(HMIPA)]·H₂O}_n (**2**)

The synthetic procedure for **2** was analogous to the synthesis of **1**: a solution of AgOAc (16.7 mg, 0.1 mmol), L2 (17.8 mg, 0.1 mmol), H₂MIPA (17.8 mg, 0.1 mmol) and H₂O (15 mL) was stirred for 0.5 h. Colorless block-shaped crystals of complex **2** suitable for X-ray diffraction were collected by mechanical separation from an amorphous solid in 25 % yield based on AgOAc. Calcd. for C₃₃H₃₈AgN₄O₅ (Fw = 678.54): C 58.4, H 5.6, N 8.3 %; found: C

Table 1 Crystallographic data for **1** and **2**

Complex	1	2
Empirical formula	C ₃₄ H ₃₀ CoN ₄ O ₄	C ₃₃ H ₃₈ AgN ₄ O ₅
Formula weight	617.55	678.54
Wavelength/Å	0.71073	0.71073
Crystal system	Monoclinic	Triclinic
Space group	<i>P</i> 2 ₁ / <i>c</i>	<i>P</i> $\bar{1}$
Unit cell dimensions		
<i>a</i> /Å	10.3963(11)	11.5143(12)
<i>b</i> /Å	16.6902(19)	11.8139(12)
<i>c</i> /Å	17.1741(19)	13.5056(14)
α /°		64.7510(10)
β /°	99.864(2)	81.7810(10)
γ /°		87.4000(9)
<i>V</i> /Å ³	2935.9(6)	1644.3(3)
<i>Z</i>	4	2
<i>D</i> _c /g·cm ⁻³	1.397	1.370
<i>F</i> (000)	1,284	702
Crystal size/mm	0.28 × 0.24 × 0.13	0.25 × 0.22 × 0.19
θ range/°	1.71–27.58	1.68–26.00
Reflections collected	17,777	9,057
Independent reflections	6,755	6,337
<i>R</i> _{int}	0.0593	0.0152
Absorption coefficient/mm ⁻¹	0.631	0.657
<i>T</i> /K	293(2)	293(2)
Goodness of fit on <i>F</i>	0.978	1.085
Final <i>R</i> , <i>wR</i> ₂ [<i>I</i> > 2σ(<i>I</i>)] ^{a,b}	<i>R</i> ₁ = 0.0483 <i>wR</i> ₂ = 0.0974	<i>R</i> ₁ = 0.0422 <i>wR</i> ₂ = 0.1210
<i>R</i> (all data) ^{a,b}	<i>R</i> ₁ = 0.1044 <i>wR</i> ₂ = 0.1183	<i>R</i> ₁ = 0.0508 <i>wR</i> ₂ = 0.1263
Largest diff. peak and hole	0.960, -0.284	1.524, -0.800

$$^a R_1 = \frac{\sum ||F_o| - |F_c||}{\sum |F_o|}$$

$$^b wR_2 = \left\{ \frac{\sum [w(F_o^2 - F_c^2)]}{\sum [w(F_o^2)]} \right\}^{1/2}$$

58.5, H 5.9, N 8.6 %. FTIR(KBr pellet, cm⁻¹): 3,501 s, 2,852 m, 1,679 s, 1,505 s, 1,385 m, 1,205 s, 832 m, 772 m, 676 m.

Catalysis experiments

The catalytic performance of complexes **1** and **2** was investigated in terms of the degradation of methyl orange, according to a typical process [27]. The catalytic degradation experiments were carried out with 150 mL (10 mg/L) methyl orange solution (the pH was adjusted to 3.0 by dropwise addition of 0.1 mol/L H₂SO₄), 50 mg of the required complex and 30 mg sodium persulfate. The experimental temperature was maintained at 30 °C, under constant stirring. The dye concentrations were measured spectrophotometrically at

Table 2 Selected bond lengths (Å) and angles (°) for **1** and **2**

Parameter	Value	Parameter	Value
[Co(L1)(IPA)] _n			
Co1–O2	2.0194(18)	O2–Co1–O4A	95.18(8)
Co1–N3	2.066(2)	N3–Co1–O4A	157.76(8)
Co1–O3A	2.0736(18)	O3A–Co1–O4A	60.80(7)
Co1–N1	2.097(2)	N1–Co1–O4A	90.31(8)
Co1–O4A	2.253(2)	O2–Co1–O1	58.82(7)
Co1–O1	2.390(2)	N3–Co1–O1	86.13(8)
O2–Co1–N3	99.03(9)	O3A–Co1–O1	107.31(7)
O2–Co1–O3A	154.25(9)	N1–Co1–O1	149.70(8)
N3–Co1–O3A	101.57(8)	O4A–Co1–O1	86.71(7)
O2–Co1–N1	91.52(8)	N3–Co1–N1	106.24(9)
O3A–Co1–N1	97.34(8)		
{[Ag(L2)(HMIPA)]·H ₂ O} _n			
Ag1–N1	2.124(3)	N1–Ag1–N3	152.45(11)
Ag1–N3	2.137(3)	N1–Ag1–O1	111.01(10)
Ag1–O1	2.551(3)	N3–Ag1–O1	94.07(10)

Symmetry transformation used to generate equivalent atoms for **1**:
A = x, -y + 1/2, z - 1/2

506 nm. This procedure was repeated in the absence of the complex as a blank comparison experiment. The degradation efficiency of methyl orange is defined as follows [28]:

$$\text{Degradation efficiency} = \frac{(C_0 - C_t)}{C_0} \times 100\%$$

where C_0 (mg/L) is the initial concentration of methyl orange, and C_t (mg/L) is the concentration of methyl orange at reaction time t (min).

X-ray crystallography

Single-crystal X-ray diffraction data for both complexes were collected on a Bruker Smart 1000 CCD diffractometer with Mo $K\alpha$ radiation ($\lambda = 0.71073$ Å) at room temperature by ω and θ scan modes. All absorption corrections were applied using the SADABS program [29]. The two structures were solved by direct methods and refined on F^2 by full-matrix least-squares techniques using the Bruker SHELXTL program package [30]. The non-hydrogen atoms were refined with anisotropic displacement parameters. The hydrogen atoms of all water molecules could be located from a difference Fourier map, while the other hydrogen atoms were included in calculated positions and refined with isotropic thermal parameters riding on the corresponding parent atoms. The crystal parameters, data collection and refinement results for complexes **1** and **2** are summarized in Table 1. Selected bond lengths and angles are listed in Table 2.

Results and discussion

Synthesis, IR spectra of complexes **1** and **2**

Both complexes were synthesized by the hydrothermal method in a H₂O system, in which the metal salt, the corresponding organic acid and the N-donor ligand were present in a molar ratio of 1:1:1. The strong and broad peak around 3,501 cm⁻¹ for **2** corresponds to the O–H stretching vibration modes of the water ligand. The peaks at 1,505–1,513 cm⁻¹ of both complexes may be attributed to $\nu_{\text{C=N}}$ of benzimidazole bands of the L1 and L2 ligands. The separation of the asymmetric and symmetric stretching vibrations of IPA²⁻ was 180 ($\nu_{\text{as}}(\text{C–O})$, 1,613 and $\nu_{\text{sym}}(\text{C–O})$, 1,433 cm⁻¹), indicating a bidentate coordination mode of the carboxylate to the metal atom [31]. A strong absorption band at 1,679 cm⁻¹ for –COOH is observed for **2**, which indicates that the carboxyl groups of the organic moieties are incompletely deprotonated [32].

Crystal structure of complex **1**

Single-crystal X-ray diffraction analysis reveals that **1** crystallizes in the monoclinic space group $P2_1/c$. The asymmetric unit of **1** contains one Co(II) atom, one L1 and one IPA²⁻ ligands. Each Co atom is hexa-coordinated, exhibiting a distorted octahedral geometry as shown in Fig. 1a. Each Co1 center is coordinated by two nitrogen atoms from two L1 ligands and four oxygen atoms from two IPA²⁻ anions. The N3, O2, O3A and O4A atoms comprise the equatorial plane (symmetry code: A: x, -y + 1/2, z - 1/2), and the two apical sites are occupied by the N and O1 atoms. The Co–N bond distances are 2.097(2) (Co1–N1) and 2.066(2) Å (Co1–N3), and the Co–O bond distances range from 2.019(2) to 2.390(2) Å, which are comparable to those of related cobalt complexes [33].

In **1**, the Co(II) atoms are connected by L1 ligands with a μ_2 -bridging mode to form a 1D zigzag chain (Fig. 1b). Neighboring 1D chains are further extended by IPA²⁻ with μ_2 - η^2 , η^2 coordination modes into a 2D layered structure. As shown in Fig. 1c, quadrangular [Co(L1)(IPA)] units can be distinguished, with their vertices occupied by four Co(II) atoms and their four sides consisting of two L1 ligands and two anionic IPA. The side lengths are 10.516(5) and 8.766(4) Å, for the L1 and IPA²⁻ ligands, respectively. From a topological perspective, when the Co(II) atom is regarded as a 4-connected node, L1 ligands and IPA²⁻ dianions can be considered as connectors, and hence, the layer can be described as a 4-connected 2D (4,4) network with (4⁴.6²) topology (Fig. 1d). Furthermore, π - π stacking interactions are observed (centroid-to-centroid distance of 3.601(2) Å) between the imidazole rings of the

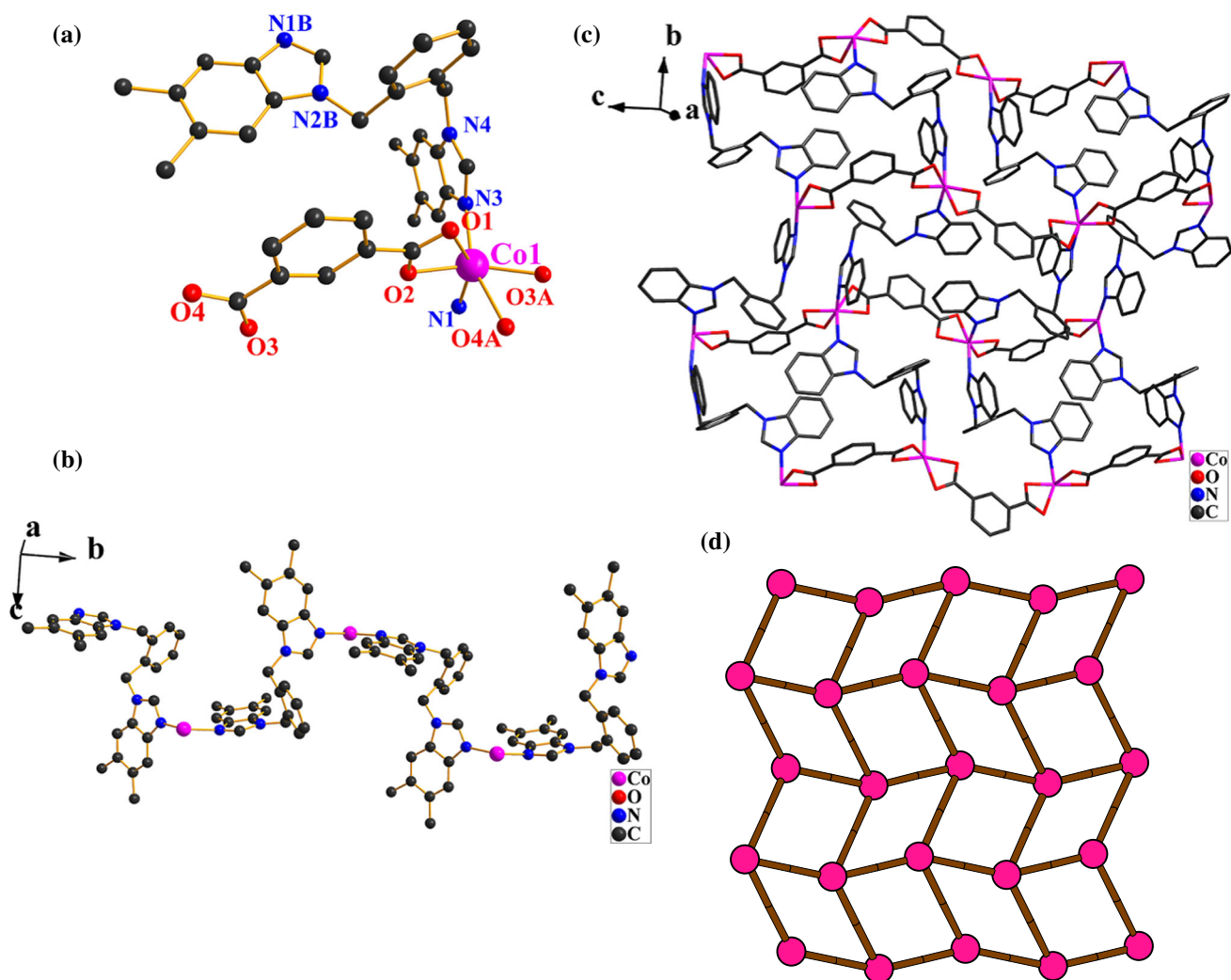


Fig. 1 **a** Coordination environment around the Co atom in **1**, all hydrogen atoms were omitted for clarity. (Symmetry codes: A : $x, -y + 1/2, z - 1/2$. B : $-x + 1, y + 1/2, -z + 3/2$); **b** View of the

1D chain constructed by L1 ligands and Co(II) ions; **c** View of the 2D supramolecular framework (methyl groups were omitted for clarity); **d** Topological view of the $\{4^4-6^2\}$ network in **1**

adjacent L1 ligands (Cg: N3–C11–C18–N14–C19), which additionally enhances the stability of the 2D network.

Crystal structure of complex **2**

Complex **2** crystallizes in the triclinic $P\bar{1}$ space group and exhibits a 1D coordination structure. The asymmetric unit of **2** consists of one Ag(I) ion, one HMIPA[−] anion, one L2 ligand and one uncoordinated water solvent molecule. Figure 2a depicts the coordination environment of the Ag(I) center, showing that it is coordinated by two nitrogen atoms from two distinct L2 ligands (Ag1–N1 = 2.124(3) Å and Ag1–N3 = 2.137(3) Å) and one oxygen atom from a HMIPA[−] dianion (Ag1–O1 = 2.551(3) Å), giving a distorted T-shaped geometry (N1–Ag1–N3 = 152.45(11)°, N3–Ag1–O1 = 94.07(10)°). Both distances of the Ag–N and Ag–O are within acceptable ranges [34, 35].

In **2**, the HMIPA[−] acts as a terminal ligand to the Ag(I) center, giving a neutral [Ag(HMIPA)] subunit. The neighboring subunits are bridged by L2 ligands to generate a 1D zigzag infinite chain structure (Fig. 2b). Each L2 ligand adopts the *anti*-configuration in which the benzimidazole rings within each unit are parallel, and the Ag1–AgA and Ag1–AgB distances are 12.871(9) and 12.976(8) Å, respectively (symmetry codes: A: $-x, -y, -z + 1$, B: $-x + 1, -y + 1, -z + 2$). Furthermore, there are two kinds of O–H...O hydrogen bond interactions (O1W...O4C = 2.830 (5) Å, O1W–H1 WB...O4C = 180(2)°, O1W...O3D = 2.842 (6) Å, O1W–H1WA...O3D = 149(6)°, symmetry codes: C: $x + 1, y + 1, z - 1$, D: $-x + 1, -y + 1, -z + 2$) between the uncoordinated lattice water molecule and symmetry-equivalent HMIPA[−] anions, resulting in a 2D supermolecule structure (Fig. 2c), which is a common network with (6³) topology (Fig. 2d). Interestingly, there are two types of π – π

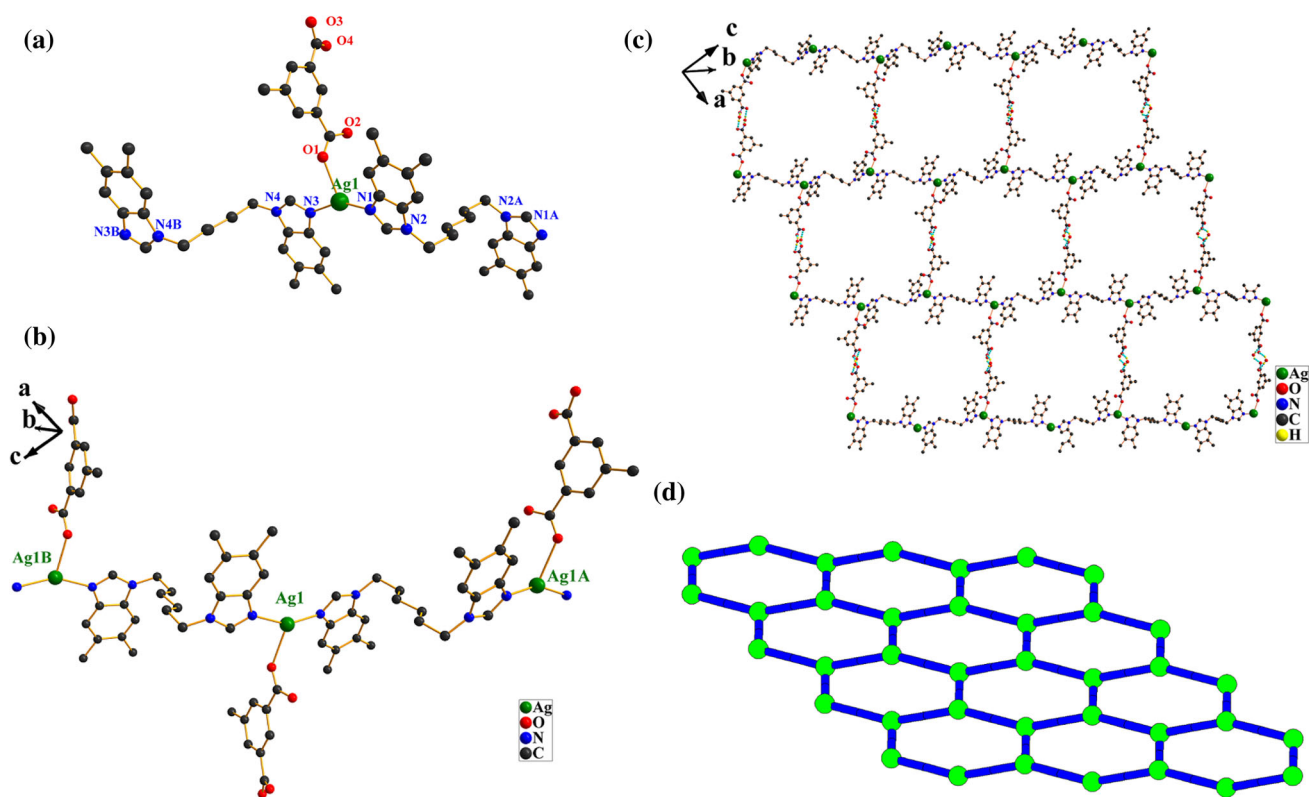


Fig. 2 **a** Coordination environment around the Ag(I) ion in **2**, all hydrogen atoms were omitted for clarity. (Symmetry codes: A : $-x, -y, -z + 1$, B : $-x + 1, -y + 1, -z + 2$); **b** 1D zigzag chain of **2**

(Symmetry codes: A : $-x, -y, -z + 1$, B : $-x + 1, -y + 1, -z + 2$); **c** 2D supramolecular network formed by O–H...O hydrogen bond interactions for **2**; **d** Topological view of the $\{6^3\}$ network in **2**

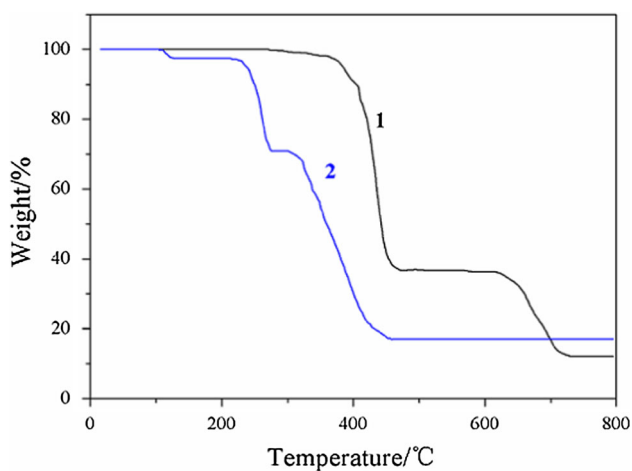


Fig. 3 TG curves for complexes **1** and **2**

stacking interaction between the benzimidazole rings of the L2 ligands, i.e., the centroid-to-centroid distances range from 3.672(3) to 3.758(5) Å (Cg1–Cg3, Cg2–Cg4, respectively), and the inter-planar angles α vary from 1.5(2) to 1.7(2)° (Cg1: N1–C1–N2–C2–C9, Cg2: N3–C22–N4–C30–C23, Cg3: C2–C3–C4–C6–C8–C9 and Cg4: C23–C24–C25–C27–C29–C30).

Thermal analysis

The thermogravimetric analysis experiments of complexes **1** and **2** were investigated under N₂ atmosphere, using a temperature gradient from room temperature to 800 °C at a rate of 10 °C/min. As shown in Fig. 3, the TG curve of complex **1** can be divided into two major steps. Complex **1** remains stable up to 260 °C, then weight loss occurs in the range of 260–477 °C, which corresponds to the release of ligand L1 (calcd: 63.6 %, found: 63.2 %). The weight loss from 573 to 727 °C can be attributed to the release of IPA²⁻ ligands (calcd: 24.3 %, found: 24.6 %). The remaining residue corresponds to CoO, which has been formed (calcd: 12.1 %, found: 12.2 %). Complex **2**, however, shows three steps in the TG curve. Firstly, the water molecules are lost from 104 to 129 °C (calcd: 2.6 %, found: 2.5 %). Secondly, the weight loss, which occurs from 213 to 276 °C, is consistent with the loss of HMIPA⁻ ligands (calcd: 26.4 %, found: 26.7 %). Thirdly, the weight loss observed from 303 to 460 °C can be assigned to the decomposition of L2 ligands (calculated: 53.9 %, found: 54.1 %). The remaining weight corresponds to Ag₂O (calcd: 17.1 %, found: 16.7 %).

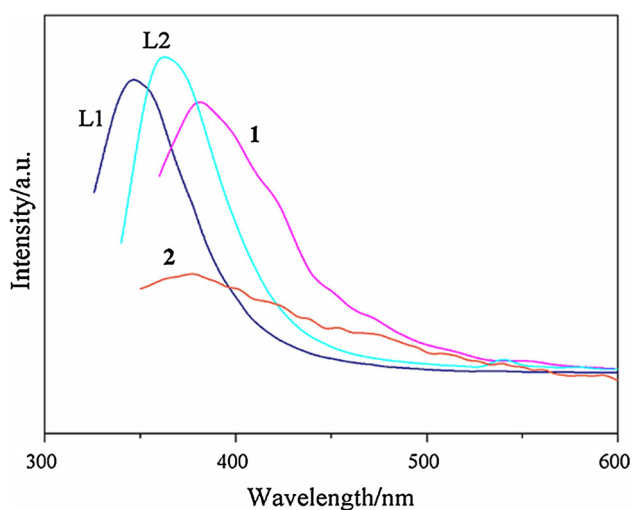


Fig. 4 Solid-state photoluminescence emission spectra of the free ligands L1, L2 and complexes **1**, **2**

Photoluminescence properties

The photoluminescence properties of **1**, **2** and free N-donor ligands L1 and L2 in the solid state at room temperature have been measured. As illustrated in Fig. 4, the free ligands L1 and L2 exhibit emission peaks at 346 and 362 nm with excitations at 298 and 320 nm, respectively. The fluorescence peaks at about 381 nm for **1** and 380 nm for **2** are found in the emission spectra upon excitation at 210 nm for both complexes. Compared with the free L1 and L2 ligands, the emission maxima of **1** and **2** are obviously red-shifted. For **1**, this might be attributed to the coordination between ligands and metal atoms. For **2**, this may come from the electronic transition between the p orbitals (filled orbitals) of coordinated N atoms and the 5 s orbital (empty orbital) of the Ag(I) center, i.e., ligand-to-metal charge transfer (LMCT), mixed with metal-centered (d-s/d-p) transitions [36]. In addition, the carboxylate ligands show very weak n- π transitions; hence, it can be considered that the carboxylate ligands do not significantly contribute to the fluorescence emission of the coordination polymers when N-donor ligands are present [37].

Catalytic degradation experiments

Azo dyes have been widely used in textile, printing, food, pharmaceutical and research laboratories because of their chemical stability and versatility [38, 39]. Most of them are non-biodegradable, toxic and potentially carcinogenic in nature. To speed up the rate of degradation, Fenton-like processes have attracted the attention of many researchers [40]. A Fenton-like process is performed under the presence of catalyst and a peroxydisulfate $S_2O_8^{2-}$, which is considered an effective oxidant system for the production

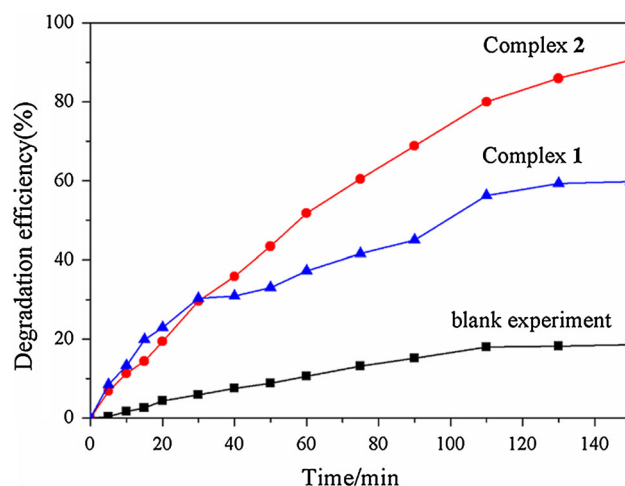


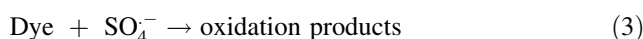
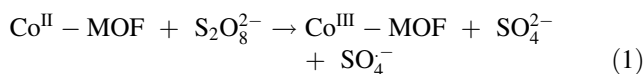
Fig. 5 Degradation experiment results

of SO_4^- , and hence, because of its strong oxidizing properties, can be used to resolve organic pollutants. As previously reported, transition metal coordination polymers can possess good catalytic properties in a Fenton-like process [41].

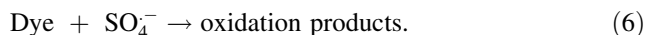
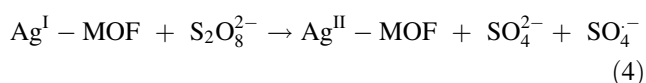
In this experiment, methyl orange was selected as a model compound, considering organic pollutants. The results of the degradation of methyl orange are depicted in Fig. 5. As is shown, when the experiment was conducted as a blank comparison test, after 150 min the degradation efficiency was only 18.2 %, indicating that methyl orange cannot be effectively oxidized by persulfate solely. However, when adding complex **1** or **2** as catalyst, the color of the methyl orange was visibly removed. The degradation efficiency of the methyl orange degradation within 30 min reaction was about 30 % in the presence of **1** and reached to approximately 60 % after 150 min. In comparison with the two above reactions, the degradation rate of the methyl orange solution increased significantly when applying **2** as the catalyst. After 150 min, the final degradation efficiency amounted up to even 90 %. Clearly, under the same conditions, the catalytic activity of **2** is higher than that of **1**. Compared with the blank comparison experiment, both of the complexes have a prominent effect on the degradation of methyl orange.

It is possible to represent the degradation mechanism, according to Eqs. (1–6), respectively.

For **1**:



For **2**:



Conclusion

In summary, two MOCs, based on flexible bis(5,6-dimethylbenzimidazole) and two kinds of benzenedicarboxylate with different substituent groups, have been synthesized under hydrothermal conditions. Complex **1** displays a 2D (4,4) network, while in complex **2**, the 1D zigzag infinite chains are converted into a 2D supramolecular layer via O–H···O interactions. The structural analysis results reveal that metal ions and the supramolecular interactions such as hydrogen bonding interactions play an important role in governing the molecular architectures. In addition, the Ag(I) complex exhibits a higher catalytic activity for the degradation of a methyl orange dye in a Fenton-like process than the Co(II) complex.

Supplementary materials

CCDC 981054 and 981055 contain the supplementary crystallographic data for the complexes **1** and **2**. These data can be obtained free of charge via <http://www.ccdc.cam.ac.uk/conts/retrieving.html> or from the Cambridge Crystallographic Data Centre, 12 Union Road, Cambridge CB2 1EZ, UK; fax: (+44) 1223-336-033; or e-mail: deposit@ccdc.cam.ac.uk.

Acknowledgments KVH thanks the Hercules Foundation (project AUGE/11/029 “3D-SPACE: 3D Structural Platform Aiming for Chemical Excellence”) for funding.

References

- Cui YJ, Yue YF, Qian GD, Chen BL (2012) *Chem Rev* 112:1126–1162
- Getman RB, Bae YS, Wilmer CE, Snurr RQ (2012) *Chem Rev* 112:703–723
- Du M, Li CP, Liu CS, Fang SM (2013) *Coord Chem Rev* 257:1282–1305
- Furukawa H, Cordova KE, O’Keeffe M, Yaghi OM (2013) *Science* 341:974–986
- Li JR, Sculley J, Zhou HC (2012) *Chem Rev* 112:869–932
- Su Z, Fan J, Okamura TA, Sun WY, Ueyama N (2010) *Cryst Growth Des* 10:3515–3521
- Li CP, Du M (2011) *Chem Commun* 47:5958–5972
- Pu AT, Yang J, Kan WQ, Yang Y, Ma JF (2013) *Polyhedron* 50:556–570
- Wang XL, Hou LL, Zhang JW, Gong CH, Liu GC (2013) *Inorg Chim Acta* 405:58–64
- Bu XH, Chen W, Hou WF, Du M, Zhang RH, Brisse F (2002) *Inorg Chem* 41:3477–3482
- Bai HY, Ma JF, Yang J, Zhang LP, Ma JC, Liu YY (2010) *Cryst Growth Des* 10:1946–1959
- Han SD, Song WC, Zhao JP, Yang Q, Liu SJ, Li Y, Bu XH (2013) *Chem Commun* 49:871–873
- Liu GC, Yang S, Wang XL, Lin HY, Tian AX, Zhang JW (2012) *Russ J Coord Chem* 38:55–60
- Liu GC, Huang JJ, Zhang JW, Wang XL, Lin HY (2013) *Transit Met Chem* 38:359–365
- Jiao CH, He CH, Geng JC, Cui GH (2012) *J Coord Chem* 65:2852–2861
- Qin L, Li YH, Ma PJ, Cui GH (2013) *J Mol Struct* 1051:215–220
- Jiao CH, Geng JC, He CH, Cui GH (2012) *J Mol Struct* 1020:134–141
- Cui GH, Li JR, Tian JL, Bu XH, Batten SR (2005) *Crys Growth Des* 5:1775–1780
- Marwaha SS, Sethi RP, Kennedy JF (1983) *Enzyme Microb Technol* 5:361–364
- Guo J, Ma JF, Liu B, Kan WQ, Yang J (2011) *Crys Growth Des* 11:3609–3621
- Liu D, Li HX, Liu LL, Wang HM, Li NY, Ren ZG, Lang JP (2010) *Cryst Eng Comm* 12:3708–3716
- Tian L, Niu Z, Yang N, Zou JY (2011) *Inorg Chim Acta* 370:230–235
- Geng JC, Liu LW, Xiao SL, Cui GH (2013) *Transit Met Chem* 38:143–148
- Xiao SL, Qin L, He CH, Du X, Cui GH (2013) *J Inorg Organomet Polym* 23:771–778
- Wang XL, Hou LL, Zhang JW, Zhang JX, Liu GC, Yang S (2012) *CrystEngComm* 14:3936–3944
- Hoskins BF, Robson R, Slizys DA (1997) *J Am Chem Soc* 119:2952–2953
- Devi LG, Kumar SG, Reddy KM, Munikrishnappa C (2009) *J Hazard Mater* 164:459–467
- Qin L, Liu LW, Du X, Cui GH (2013) *Transit Met Chem* 38:85–91
- Sheldrick GM (1996) SADABS, program for empirical absorption correction of area detector data. University of Göttingen, Germany
- Sheldrick GM (2008) *Acta Cryst A* 64:112–122
- Deacon GB, Phillips RJ (1980) *Coord Chem Rev* 33:227–250
- Gu XJ, Xue DF (2006) *Cryst Growth Des* 6:2551–2557
- Qin L, Xiao SL, Ma PJ, Cui GH (2013) *Transit Met Chem* 38:627–633
- Du JL, Hu TL, Zhang SM, Zeng YF, Bu XH (2008) *CrystEngComm* 10:1866–1874
- Wang CC, Wang P, Guo GS (2010) *Transit Met Chem* 35:721–729
- Sun D, Zhang N, Huang RB, Zheng LS (2010) *Cryst Growth Des* 10:3699–3709
- Li YW, Ma H, Chen YQ, He KH, Li ZX, Bu XH (2012) *Cryst Growth Des* 12:189–196
- Haqea E, Lee JE, Jang IT, Hwang YK, Chang JS, Jegal J, Jung SH (2010) *J Hazard Mater* 181:535–542
- Xu XR, Li XZ (2010) *Sep Purif Technol* 72:105–111
- Ateer BM, Beattie N, Richens DT (2013) *Inorg Chem Commun* 35:284–289
- Xiao SL, Liu YG, Qin L, Cui GH (2013) *Inorg Chem Commun* 36:220–223